Separation Science and Technology
Publication details, including instructions for authors and subscription information:
http://www.informaworld.com/smpp/title~content=t713708471

Adsorption of Phenol and Basic Dye on Carbon Nanotubes/Carbon Fabric Composites from Aqueous Solution

Jung-Pin Wang[a]; Hsi-Chi Yang[b]; Chien-Te Hsieh[c]
[a] Ph.D. Program of Technology Management, Chung Hua University, Hsinchu, Taiwan [b] Department of Construction Management, Chung Hua University, Hsinchu, Taiwan [c] Department of Chemical Engineering and Materials Science, Yuan Ze Fuel Cell Center, Yuan Ze University, Taoyuan, Taiwan

Online publication date: 18 January 2011

To cite this Article Wang, Jung-Pin , Yang, Hsi-Chi and Hsieh, Chien-Te(2011) 'Adsorption of Phenol and Basic Dye on Carbon Nanotubes/Carbon Fabric Composites from Aqueous Solution', Separation Science and Technology, 46: 2, 340 — 348
To link to this Article: DOI: 10.1080/01496395.2010.508066
URL: http://dx.doi.org/10.1080/01496395.2010.508066

Separation Science and Technology, 46: 340–348, 2011

ISSN: 0149-6395 print/1520-5754 online
DOI: 10.1080/01496395.2010.508066

Taylor & Francis
Taylor & Francis Group

Adsorption of Phenol and Basic Dye on Carbon Nanotubes/ Carbon Fabric Composites from Aqueous Solution

Jung-Pin Wang,[1] Hsi-Chi Yang,[2] and Chien-Te Hsieh[3]

[1]*Ph.D. Program of Technology Management, Chung Hua University, Hsinchu, Taiwan*
[2]*Department of Construction Management, Chung Hua University, Hsinchu, Taiwan*
[3]*Department of Chemical Engineering and Materials Science, Yuan Ze Fuel Cell Center, Yuan Ze University, Taoyuan, Taiwan*

The liquid-phase adsorption of phenol and dye (basic violet 10) onto carbon nanotube (CNT)-activated carbon fabric (ACF) composites, prepared by a catalytic chemical vapor deposition (CCVD) approach, has been investigated. The CCVD technique enables the decoration of CNTs on microscaled ACFs, creating a hierarchy CNT-ACF composite. The as-grown nanotubes were found to have a tortuous shape and to be several micrometers in length. The deposition of CNTs efficiently shifts the micropore size distribution of ACFs to mesoporosity. The adsorption isotherms for phenol and BV10 on ACF and CNT-ACF adsorbents are well characterized by the Dubinin-Radushkevich and Langmuir models. The surface accessibility, the equilibrium rate constant, and the adsorption energy are significantly enhanced due to the deposition of CNTs, as analyzed by these models. Accordingly, the existence of CNTs on ACF adsorbent plays a positive role in facilitating pore accessibility to adsorbate and providing more adsorptive sites for the liquid-phase adsorption.

Keywords activated carbon fabrics; adsorption; basic dye; carbon nanotubes; chemical vapor adsorption; phenol

INTRODUCTION

The adsorption of pollutant compounds from the liquid phase is one of the most efficient approaches in drinking water and wastewater treatments, and has been extensively investigated in literature (1–6). Activated carbon (AC) and activated carbon fabric (ACF) are popular adsorbents because they exhibit a large surface area and pore volume, which allow the removal of liquid-phase contaminants, including organic compounds, heavy metal ions, and colors (7,8). The criterion for determining whether to use the treatment is often the adsorption capacity of carbon adsorbents relative to alternative treatment processes (9). More recently, an alternative carbon structure, carbon nanotube (CNT), has attracted considerable attention due to its unique chemical structure and intriguing physical properties. CNTs are considered to be promising adsorbents, and numerous studies have demonstrated their potential in adsorption and drinking water treatments, such as the removal of metallic ions and organic compounds from the liquid phase (10–13).

It is generally recognized that adsorption capacity is crucial in the selection of suitable adsorbents for removing contamination from the liquid or vapor phase. The removal efficiency of adsorbents usually depends on surface characteristics, such as porosity and pore size distribution. Basically, commercial AC or ACF generally possesses a surface area of 800–1500 $m^2\ g^{-1}$, which is much higher than that of fresh CNTs (*ca.* 120–220 $m^2\ g^{-1}$) (14,15). It has been shown that the amount of adsorbed organic compounds in the liquid phase generally increases with the surface area of ACs. However, the adsorption capacity is not proportional to the surface area of ACs derived from the same precursor (16,17). This finding indicates that the affinity of carbon surface to adsorbates (the accessibility of adsorbate into micropores or mesopores) is strongly affected by the pore size distribution; that is, not all porous structures of carbon are favorably accessible to contamination compounds in the liquid phase (18). Accordingly, the capacities of carbon for contaminant compounds are significantly affected by the pore structures of ACs or ACFs as well as the size of the adsorbate. However, there are few reports that focus on modifying AC or ACF adsorbents by using the deposition of CNT branches.

Polyacrylonitrile (PAN)-based ACFs have been demonstrated to display an excellent capability on the removal efficiency of several organic compounds (19–22). In fact, ACFs have been applied in a variety of practical applications due to their huge adsorption volume, heat-resistance, acid-proof, and base-proof capabilities. ACFs also show significant removal ability in adsorbing bacteria, organic vapor, inorganic gas, inorganic gas as well as substances

Received 13 April 2010; accepted 9 July 2010.
Address correspondence to Chien-Te Hsieh, Department of Chemical Engineering and Materials Science, Yuan Ze Fuel Cell Center, Yuan Ze University, Taoyuan 320, Taiwan, Republic of China. Tel.: +886-3-4638800 ext. 2577; Fax: +886-3-4559373. E-mail: cthsieh@saturn.yzu.edu.tw

in water solution, comparing with granular ACs. The surface area of the PAN-based ACF is mainly contributed by micropores (pore size <2 nm) that are suitable for adsorbing small liquid-type contaminants (23). Our previous studies (24,25) have proposed the use of the catalytic chemical vapor deposition (CCVD) technique to grow high-density CNTs that attach to PAN-based ACFs. It is known that CNTs have a dispersion problem and tend to easily aggregate together, forming a loose aggregation. Thus, it is very difficult to apply in adsorption tower in industry or adsorption column in drinking water and purification systems. One way to resolve the above problem is to directly grow nanoscaled CNTs on microscaled carbon matrix. Thus, incorporating with ACF and CNT, such unique carbon composites are expected to be excellent adsorbents. This is because the ACF act as a stable carbon matrix, and the appearance of CNTs not only provides additional active sites but also shifts the pore size distribution, reducing the effect of pore blocking on microporous channels. Two types of adsorbates, phenol (molecular formula: C_6H_5OH, molecular weight (MW): 94) and basic violet 10 (BV10, molecular formula: $C_{28}H_{31}ClN_2O_3$; MW: 478.5) are used as target organic pollutants for adsorption experiments. Phenol and its derivatives are frequently encountered in wastewater treatment, and the capacity for phenol thus serves as an important indicator for the adsorption of polar aromatic compounds of small sizes (18). The capacity of BV10 can be considered as an index for removing larger molecules from the liquid phase. A series of adsorption experiments were carried out and the resulting adsorption isotherms were interpreted by using well-developed models, i.e., Langmuir and Dubinin-Radushkevich (D-R) models.

EXPERIMENTAL

Synthesis of CNT-ACF Composites

A similar CCVD procedure for fabricating CNT-ACF composites has been reported elsewhere (24,25). A brief description can be illustrated as follows. The PAN-based ACFs (Taiwan Carbon Technology Co., Taiwan) used in this study have a cloth-like form consisting of regularly mircoscaled carbon fibers. This fabric has a thickness of 0.4–0.6 mm, and the diameter of each carbon fiber in the fabric is approximately 8–10 μm. A fresh ACF sample was chemically oxidized by nitric acid washing at 85°C, allowing the implantation of surface oxides on the ACF surface. We placed a 0.5 g oxidized ACF sample into a 0.5 M nickel nitrate solution, and then the carbon-based slurries were stirred under N_2 atmosphere at ambient temperature for 6 hr. After filtration, a direct heating process was performed at 350°C under an H_2 atmosphere, giving the Ni-attached ACFs. The CCVD technique was used to grow CNT branches on Ni-attached fabric using a mixture of a carbon precursor (N_2:H_2:C_2H_2 = 94:1:5 in v/v/v). The vapor-growth process was carried out in a vertical furnace at 850°C for a growth period of 1 hr, thus forming CNT/ACF adsorbents.

Characteristics of CNT-Based Adsorbents

Porous characterizations of the CNFs were determined by N_2 adsorption at −196°C using an automated adsorption apparatus (Micromeritics ASAP 2010). The specific surface areas and porosities of these carbons were determined by gas adsorption. Before any such analysis the carbon sample was degassed at 120°C in a vacuum at about 10^{-3} Torr. The surface areas and micropore volumes of the samples were determined from the application of the Brunauer-Emmett-Teller (BET) and D-R equations, respectively, to the N_2 adsorption isotherms at relative pressures of between 0.06 and 0.2. The density functional theory (DFT) method was used to analyze the pore size distribution (i.e., 1–100 nm). The morphological observation for the carbon composites was characterized by field-emission scanning electron spectroscopy (FE-SEM, JEOL JSM-5600) and transmission electron microscopy (TEM, JEOL JEM-6500 F).

Liquid-Phase Adsorption Experiments

As stated in the preceding section, phenol and BV10 were used as adsorbates in the liquid-phase adsorption experiments. The preparation of the various solutions in this study was done as follows. The organic compounds, phenol (1000 mg L^{-1}) and BV10 (200 mg L^{-1}), were prepared by diluting the adsorbates in distilled water. Adsorption experiments were conducted by placing a certain amount of ACF adsorbents and 100 cm^3 of the prepared aqueous solution into a 250 cm^3 glass-stoppered flask. The flask was put in a constant-temperature shaker bath at 30°C, with a shaker speed of 100 rpm. Preliminary experiments had shown that the adsorption process attained equilibrium in 12 hr for all the carbon samples used in the present study.

Upon equilibration, all samples were passed through nylon filters prior to analysis in order to minimize the interference of carbon fines with the analysis. The concentrations of the adsorbates in the residual solutions were analyzed by a UV/visible spectrophotometer (Shimadzu, Model UV-2550) at appropriate wavelengths. Phenol and BV10 absorb ultraviolet radiation at $\lambda = 268$ and 555 nm respectively. The concentrations were measured by comparing the light absorbance of the sample solutions against a standardization curve prepared for each compound. The amount of adsorbate captured by the adsorbers was determined as follows:

$$Q_e = \frac{(C_i - C_e)V}{M} \quad (1)$$

where Q_e is the amount of the adsorbate on the carbon at equilibrium, C_i is the initial concentration of the adsorbate in the aqueous solution, C_e is the residual concentration, V is the volume of the aqueous solution, and M is the amount of carbon used in the adsorption.

RESULTS AND DISCUSSION

Porous Characteristics of ACF Adsorbents

Figure 1(a) shows the FE-SEM image for fresh ACF adsorber consisting of a number of microscaled carbon fibers. It can be seen from the figure that each fiber, with an average size of 8 μm, has a smooth and clean surface. Figures 1(b) and (c) show the FE-SEM images for fresh ACF decorated with CNTs (i.e., CNT-ACF), prepared through the CCVD technique, at low and high magnifications, respectively. The CNTs were uniformly grown in microsized carbon fibers, thus generating a hierarchy CNT-ACF composite. Generally, as-grown nanotubes were found to have a tortuous shape and to be several micrometers in length. Since as-deposited Ni nanoparticles randomly decorate some defects of the ACF surface, they thus provide a number of catalyzed sites in depositing the graphene layers at different axes. The description of the growth mechanism of carbon heterojunctions has been reported in previous studies (23,24). A typical TEM observation of the inner morphology of individual CNTs is shown in Fig. 1(d). The nanotubes are typically hollow along a one-dimensional shape, without any blockage of metallic catalysts. Each nanotube displays an average outer diameter of *ca*. 20–40 nm and a tube thickness of 2–5 nm. Accordingly, the tubular type of as-grown CNTs generally contributes to the mesoporous volume.

The surface characteristics of ACFs determined from N_2 isotherms are shown in Table 1. Data from this table, a fresh ACF sample, shows a fairly high BET surface area of 1065 $m^2\ g^{-1}$ and total pore volume of 0.52 $cm^3\ g^{-1}$. The decoration of CNTs tends to lower the porosity of the ACF adsorber, i.e., a decrease in the BET surface area from 1065 to 565 $m^2\ g^{-1}$. The ACF adsorber is mainly microporous with 95% micropore fraction, whereas the mesopore fraction in CNT-ACF displays an obvious increase (mesopore fraction: 31%). This improvement in mesopore volume can be ascribed to the fact that the attachment of nanotubes to microporous ACF matrix shifts the pore size distribution to the mesopore region since as-grown CNTs are mostly mesoporous. The DFT approach was applied to analyze the pore size distribution, as shown in Fig. 2. In comparison, the original ACF displays a narrow micropore size distribution (1 nm <pore size <2.5 nm), whereas CNT-ACF shows a broad distribution ranging from 1 nm to 10 nm. The shift in the pore size distribution is attributed to

(i) as-grown CNTs having opened tips and a mesoporous tubular shape, and
(ii) an aggregation of CNTs, which possibly contributes to the interspaces between the nanotubes, thus improving the fraction of mesopore.

Additionally, it is worth noting that the intensity of the micropore peak becomes weak. This is presumably due to

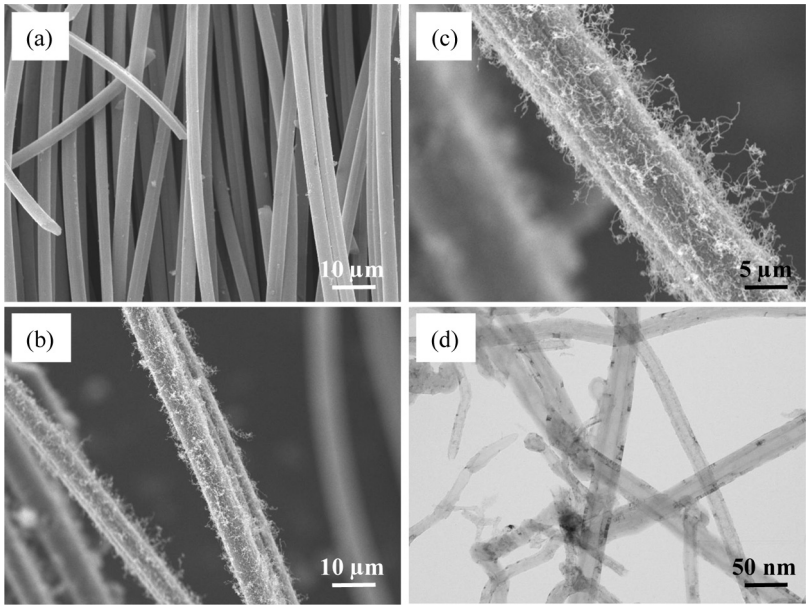

FIG. 1. FE-SEM images of (a) fresh ACF and CNT-ACF samples with (b) low and (c) high magnifications. (d) TEM image for as-grown CNTs, prepared by CCVD method using ethylene and Ni as carbon precursor and catalyst, respectively.

TABLE 1
Surface characteristics of original ACF and ACF decorated with CNTs (CNT-ACF)

Carbon type	Specific surface area ($m^2\ g^{-1}$)		Pore volume ($cm^3\ g^{-1}$)		
	S_{BET} [a]	S_t [b]	V_t [c]	V_{micro} [d] (%)	V_{meso} [e] (%)
ACF	1065	1155	0.52	0.49 (95)	0.03 (5)
CNT-ACF	565	619	0.36	0.25 (69)	0.11 (31)

[a] S_{BET}: specific surface area computed using BET equation.
[b] S_t: specific surface area determined by *t*-plot method.
[c] V_t: total pore volume estimated at a relative pressure of 0.98.
[d] V_{micro}: micropore volume determined from the Dubinin-Radushkevish equation.
[e] V_{meso}: mesopore volume determined from the subtraction of micropore volume from total pore volume.

one reason that some portion of interior channels in ACF is presumably hindered from the deposition of CNTs or Ni catalysts.

Adsorption Isotherms of ACF Adsorbents

To ensure adsorption equilibrium, the adsorption kinetics of phenol and BV10 on different adsorbents have been carried out, as shown in Fig. 3(a) and 3(b). As to the adsorption of phenol, both ACF and CNT-ACF shows a rapid rate to attain the equilibrium, i.e., ~3 hr. However, the equilibrium period for the adsorption of BV10 on CNT-ACF takes *ca.* 4 hr, which is much shorter than that for ACF (~7 hr). Since BV10 has the larger molecular size than phenol, the passage-providing role played by mesoporous CNTs in facilitating the access of adsorbates to interior micropores thus becomes more influential, resulting in the fact that CNT-ACF has a much higher adsorption rate than ACF. On the basis of the adsorption kinetics, both the adsorbate size and adsorber type would act a crucial role in determining the adsorption behavior. This finding can be supported by the effect of diffusion resistance, depending on the molecular size and the pore structure of the adsorber. The decoration of CNTs strongly facilitates the molecular accessibility to the ACFs, demonstrated by the adsorption kinetics of BV10. This can be attributed to the fact that the presence of CNTs on exterior ACF has a short diffusion path and provides excess outer active sites for adsorption of adsorbates in liquid phase.

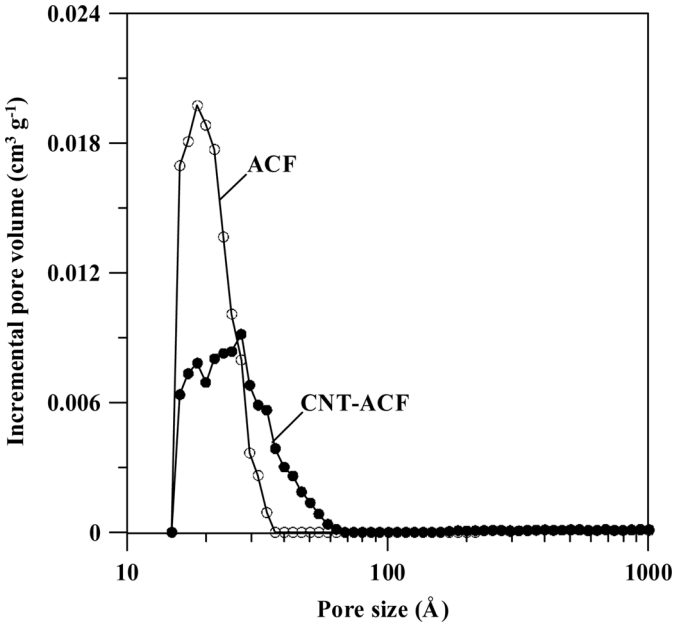

FIG. 2. Pore size distributions of fresh ACF and CNT-ACF adsorbents, determined from DFT method.

The equilibrium adsorption isotherms of phenol onto ACF and CNT-ACF adsorbers in aqueous solutions are shown in Figs. 4 and 5, respectively, i.e., the relationship between the amount of phenol adsorbed per unit mass of carbon and their remaining concentrations in the aqueous solutions (16). Generally, in the range of equilibrium concentration, both adsorption isotherms reflect that the phenol amount adsorbed on the ACF surface are of monolayer (Langmuir) type. The adsorption capacities are compared to show a slight decrease after the decoration of CNTs. This finding shows that the influence of CNT decoration on the adsorption capability of phenol seems to be minor. Figures 5 and 7 show the adsorption isotherms of BV10 onto ACF and CNT-ACF, respectively. As with phenol adsorption, the adsorption isotherms for BV10 exhibit Langmuir-type behavior. At a specified concentration, the equilibrium adsorption capacity of CNT-ACF is much higher than that of ACF. It is generally recognized that the BET surface area is a crucial factor in determining the adsorption capacities of adsorbents (1). However, as for the adsorption of BV, the surface area available for BV10 adsorption is not proportional to the adsorption capacity onto ACF adsorbers. This result can be inferred from the fact that various pore sizes and carbon types lead to surface heterogeneity, thus affecting the adsorption behavior.

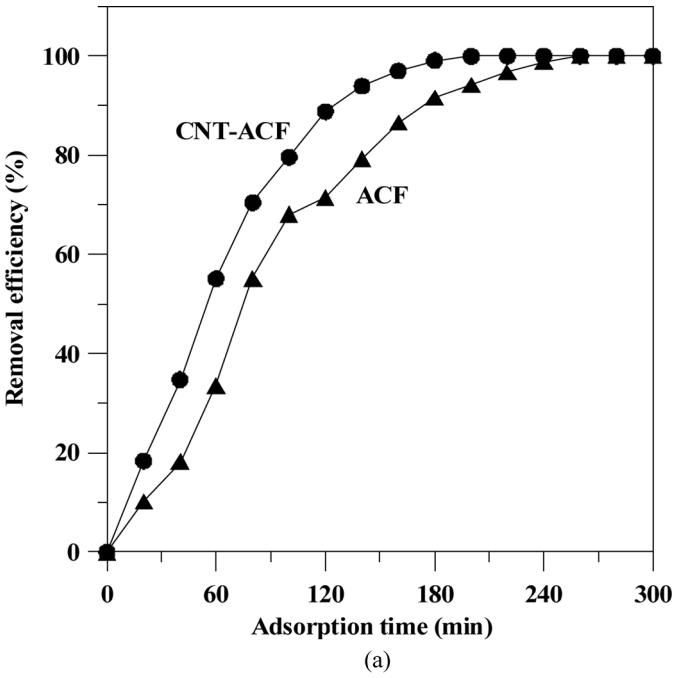

(a)

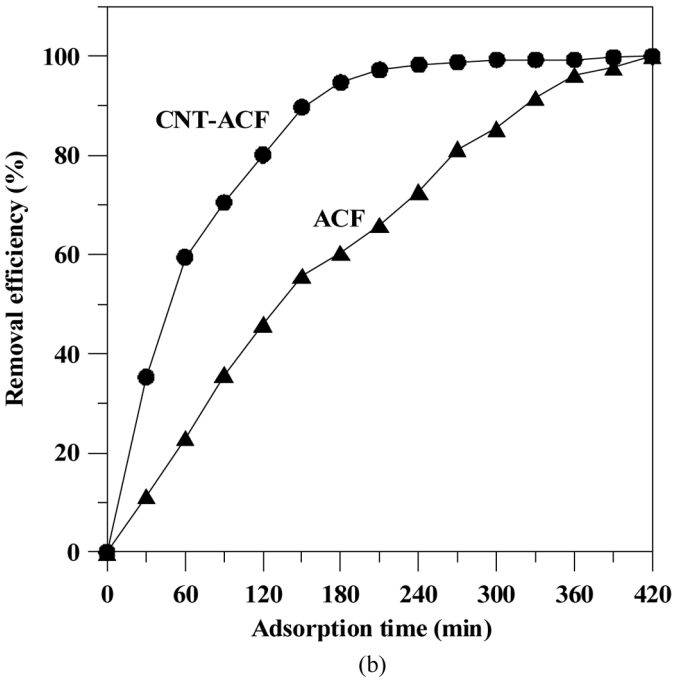

(b)

FIG. 3. Adsorption kinetics of (a) phenol and (b) BV10 on ACF and CNT-ACF adsorbents at 30°C.

Our previous study has pointed out that surface heterogeneity is strongly affected by pore size distribution (17). Basically, micropores serve as the major providers of adsorptive sites in aqueous solutions, whereas only weaker adsorption is observed in mesopores (18). It is generally believed that adsorption on porous carbon proceeds through a sequence of diffusion steps from the bulk phase into mesopores and then to micropores. The longer the diffusion path of micropores, the more difficult achieving complete saturation of carbon adsorbers becomes, since

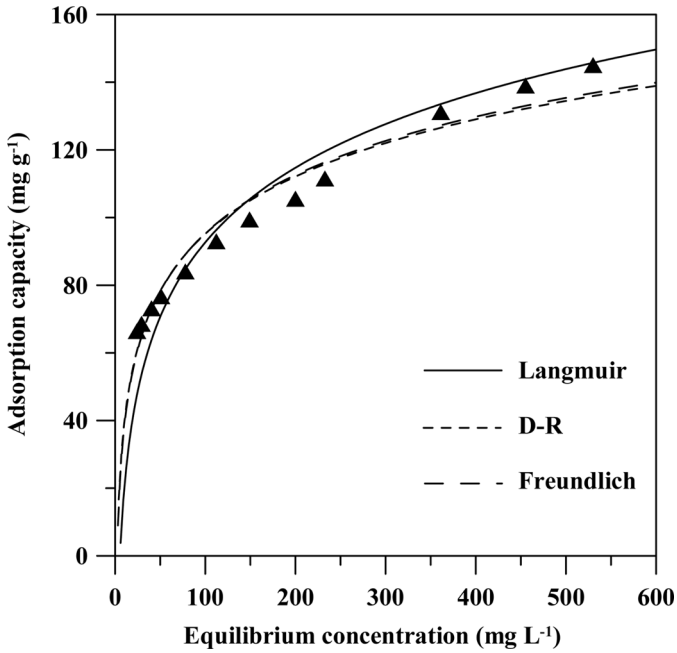

FIG. 4. Adsorption isotherm of phenol on ACF adsorbent at 30°C, in which the solid symbols are experimental data and three prediction curves are Langmuir, D-R, and Freundlich equations.

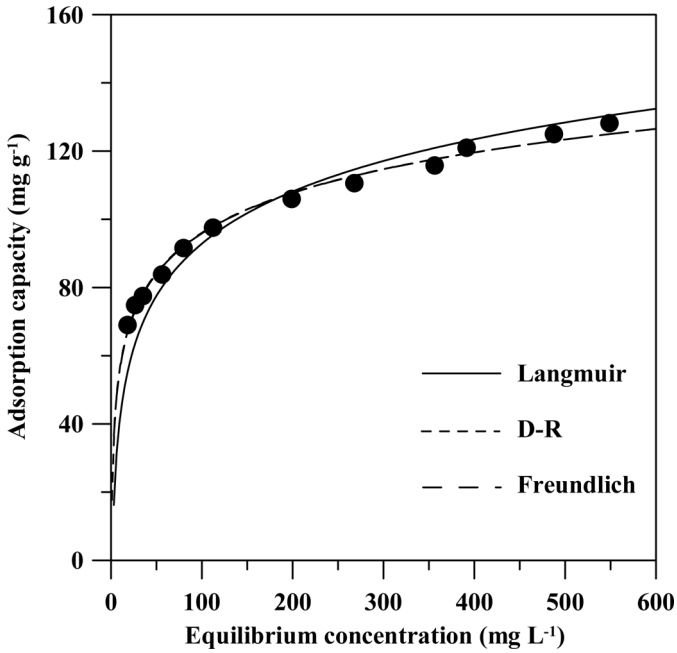

FIG. 5. Adsorption isotherm of phenol on CNT-ACF adsorbent at 30°C, in which the solid symbols are experimental data and three prediction curves are Langmuir, D-R, and Freundlich equations.

the probability that the adsorbate molecules will come up against pores too small for the adsorbate to penetrate will be greater (7,26). Under this circumstance, mesopores would play the role of providing adsorbates an easy access to the interior micropores in carbons. Thus it can be clarified that some of the micropore entrances in ACF adsorbent are blocked by one or more adsorbed molecule easily, preventing the adsorption of phenol molecules to the surface within the blocked pores. This influence of pore blockage becomes more evident especially for the adsorption of molecules (e.g., BV10) with large sizes. On the other hand, the decoration of CNTs would provide an exterior surface area accessible for liquid-phase adsorption even if CNT-ACF possesses a smaller microporous surface area; that is, CNT-ACF contains a large number of new mesopore channels, thus preventing pore blockage from the diffusion path of micropores and allowing adsorbates to penetrate.

Additionally, it is generally recognized that the micropores of carbons cannot be fully wetted in aqueous solutions and thus are not fully accessible to adsorbate molecules in the liquid phase. The wetting property would dramatically affect the surface coverage for the adsorption of phenol and BV10. It can happen easily in this case if the carbon adsorbers were more microporous. Since the CNTs grow on the outer surface of ACF, the CNT-ACF adsorbent consists of more additional sites available for the occupancy of adsorbates. It is believed that there are five types of adsorptive sites on as-grown CNTs, including inner cavities, interstitial channels, both ends, ridges, and the aggregate's outer surfaces (27–30). These outer active sites are easily accessible to the penetration of adsorbates, inducing a higher adsorptive coverage in the liquid phase. Further investigation would apply adsorption models to explore how the available surface area affects liquid-phase adsorption in ACF adsorbents.

Analysis of Isotherms by Adsorption Models

Two two-parameter isotherm equations, D-R and Langmuir, are applied for further interpretation of the adsorption data obtained in the preceding section. The correlation of equilibrium data with a theoretical equation giving a satisfactory description of the adsorption in the liquid phase would offer a clue to the key mechanistic steps in the overall adsorption process. For comparison, one empirical model, the Freundlich equation, is also applied to compare with the experimental data, as shown in Figs. 4–7.

In deriving the D-R equation for liquid-phase adsorption, the amount adsorbed corresponding to any equilibrium concentration is assumed to be a Gaussian function of the Polanyi potential (18,31–34), ε,

$$Q_e = Q_{DR} \exp[-b\varepsilon^2] \quad (2)$$

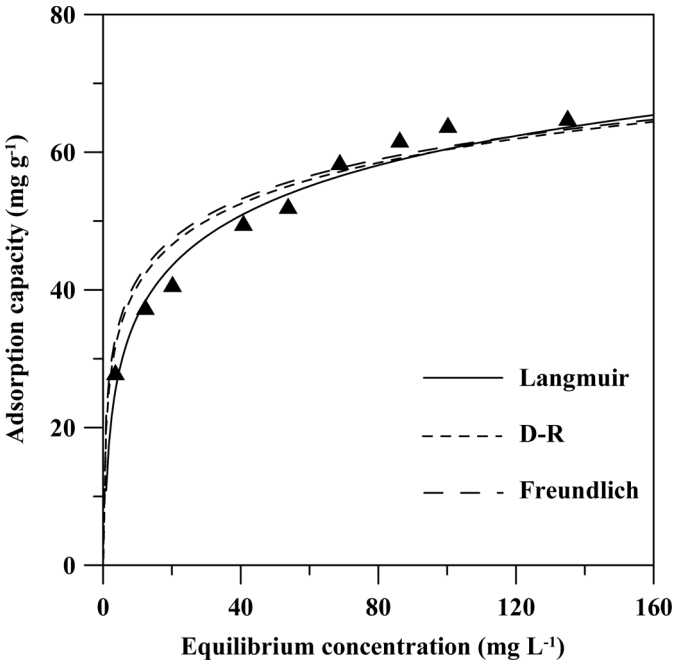

FIG. 6. Adsorption isotherm of BV10 on ACF adsorbent at 30°C, in which the solid symbols are experimental data and three prediction curves are Langmuir, D-R, and Freundlich equations.

with

$$\varepsilon = RT \ln(1 + \frac{1}{C_e}) \quad (3)$$

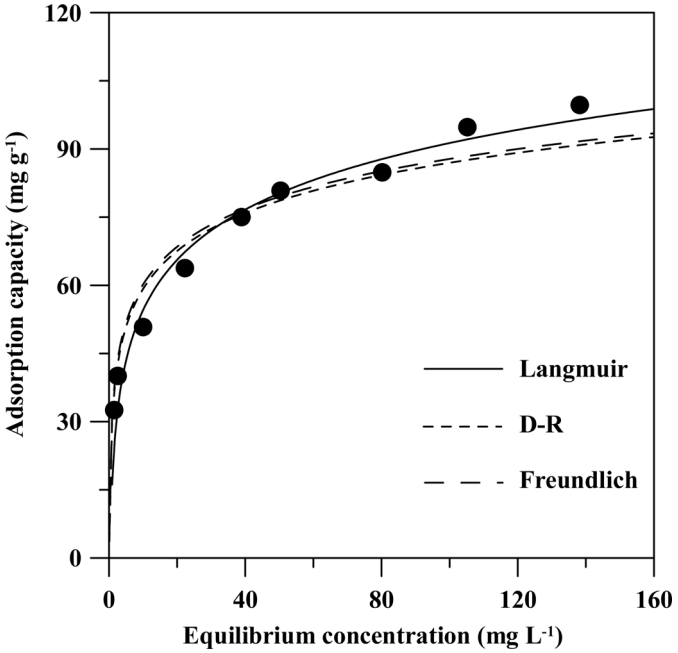

FIG. 7. Adsorption isotherm of BV10 on CNT-ACF adsorbent at 30°C, in which the solid symbols are experimental data and three prediction curves are Langmuir, D-R, and Freundlich equations.

TABLE 2
The most suitable parameters of Dubinin-Radushkevich isotherms for adsorption of phenol and BV10 onto carbon adsorbents at 30°C

Carbon type	Q_{DR} (mg g^{-1})	E (kJ mol^{-1})	r^2
Phenol adsorption			
ACF	307.0	15.0	0.971
CNT-ACF	217.5	18.1	0.995
BV10 adsorption			
ACF	162.4	16.7	0.988
CNT-ACF	220.0	17.2	0.977

where Q_{DR} is the maximal capacity of adsorbates on ACFs, and B is a constant related to the adsorption energy. The most probable free energy of adsorption is

$$E = \frac{1}{\sqrt{2B}} \tag{4}$$

Therefore, the use of the D-R equation results in an estimation of the maximum adsorption capacity as well as an average free energy value unique to the adsorbate-adsorbent system (18). A linearity plot of ln Q_e against ε^2 would give the values of Q_{DR} and B from the intercept and slope, respectively. Thus the mean free energy of adsorption, E, can be determined by substituting the B value into Eq. (). The parameters for the D-R equation as well as the r^2 value are shown in Table 2. The simulation curves, determined from the data on Table 2, are also given and compared with the experimental data (see Figs. 4–7), and show a fairly good fit to these adsorption isotherms.

Basically, the magnitude of the E value can be considered as an estimate of the adsorption mechanism (31). It can be seen from the data on Table 2 that the adsorption energies fall into the regions of 15.0–18.1 and 16.7–17.2 kJ mol^{-1} for phenol and BV10 adsorption, respectively. This suggests that these adsorption behaviors originate from a chemical ion-exchange reaction rather than physical adsorption. This analysis also indicates that the existing CNTs tend to enlarge the E value. This improvement of the E value can be possibly attributed to an increasing mesopore fraction, again indicating that mesoporous nanotubes enable the adsorbates to access to the inner and narrow micropores, the walls of which provide overlapping potentials to increase the free energy for adsorption (9). The energy analysis also indicates the crucial role that the presence of CNTs plays in the liquid-phase adsorption.

The most widely used two-parameter equation is the Langmuir equation, which is expressed as (35,36)

$$Q_e = \frac{Q_L K_L C_e}{1 + K_L C_e} \tag{5}$$

where Q_L is the amount of adsorbate adsorbed per unit mass of carbon corresponding to complete monolayer coverage, and K_L is the Langmuir constant, which can be considered as a measure of adsorption energy (7). A linear plot of (C_e/Q_e) against C_e was used to give the values of Q_L and K_L from the slope and intercept of the plot. These parameters, together with the r^2 value, of the Langmuir equation for the adsorption of phenol and BV10 onto different adsorbers are shown in Table 3. The Langmuir equation also offers a fairly good fit to phenol and BV10 isotherms, as shown in Figs. 4–7.

From the data on Table 3, it is apparent that the monolayer adsorption capacity does not display a linear increase with increasing the BET surface area. This finding indicates that the total microporosity of ACF cannot be fully accessed by the adsorbate molecules, especially for large adsorbates. However, as-produced CNTs offer more attractive sites, including grooves between adjacent tubes on the perimeter of the bundles, accessible interstitial channels, and external nanotube walls (30). Therefore, the appearance of CNTs plays a positive role in

(i) facilitating the pore accessibility to adsorbates and
(ii) providing more adsorptive sites for the liquid-phase adsorption.

Theoretically, the value of Q_L represents a limited number of sites that are capable of adsorbing adsorbates. The maximal coverage of carbons for phenol and BV10 adsorption can be examined, by assuming that the BET surface area can be occupied by the adsorbates. Therefore, the surface coverage (X_m) of the BET area covered by the adsorbates can be determined according to Q_L and the X_m values are also shown in Table 3. This difference between the X_m values is due to an integrated effect of the adsorbate size and pore size distribution. Since BV10 molecules have a larger size than those of phenol, achieving complete saturation of ACFs becomes more difficult.

TABLE 3
The most suitable parameters of Langmuir isotherms for adsorption of phenol and BV10 onto carbon adsorbents at 30°C

Carbon type	Q_L (mg g^{-1})	K_L (L mg^{-1})	r^2	X_m (%)
Phenol adsorption				
ACF	155.0	0.0165	0.981	28.1
CNT-ACF	131.1	0.0317	0.996	44.8
BV10 adsorption				
ACF	70.0	0.0816	0.992	12.4
CNT-ACF	103.1	0.0879	0.983	34.5

Thus, adsorption of large adsorbates, such as BV10, would suffer a more serious pore blockage in microporous channels. In contrast, this influence is less significant for phenol adsorption on ACF adsorbents. The data on Table 3 also prove that the existence of CNTs significantly promotes the values of X_m for the adsorption of both phenol (X_m: 44.8%) and BV10 (X_m: 34.5%), thus showing the importance of the existence of CNTs. This can be attributed to the fact that the deposition of CNTs on the ACF surface donates a number of available sites that offer a strong affinity for the adsorption of phenol and BV10 in the liquid phase. This argument can be supported by the fact that CNT-ACF adsorbent displays higher K_L values than those of ACF. This reflects an enhanced forward adsorption in the reversible reaction due to the deposition of CNTs, thus leading to better pore accessibility.

CONCLUSIONS

Liquid-phase adsorption of phenol and BV10 onto CNT-ACF adsorbent was conducted to explore the influence of the deposition of CNT on the adsorption capacity. A large amount of CNTs was attached to microscaled carbon fibers by the CCVD approach that used Ni and ethylene as catalyst and carbon precursor, respectively. The as-grown nanotube displays an average outer diameter of *ca*. 20–40 nm and a tube thickness of 2–5 nm. The deposition of CNTs was found to efficiently alter the pore size distribution of ACFs, shifting to mesoporosity. Adsorption isotherms for phenol and BV10 on ACF and CNT-ACF adsorbents were well characterized by three types of adsorption models: Freundlich, D-R, and Langmuir. The analyzed results clearly showed that the appearance of CNTs leads to surface heterogeneity, significantly affecting the liquid-phase adsorption behavior. Both the equilibrium rate constant (Langmuir) and the adsorption energy (D-R) display an increase due to the decoration of CNTs, inducing higher surface coverage for the adsorption of BV10 adsorbates. This reflects that CNT-ACF contains a large number of mesopore channels, thus preventing the pore blockage from the diffusion path of micropores for adsorbates to penetrate. Accordingly, the appearance of CNTs on ACF adsorbent plays a positive role in

(i) facilitating the pore accessibility to adsorbate and
(ii) providing more adsorptive sites for the dye adsorption in liquid phase.

ACKNOWLEDGEMENTS

The authors gratefully acknowledge financial support from the Ministry of Education (MOE) and the National Science Council (NSC) in Taiwan, through Project No.: NSC 97–2221-E-155–031-MY2.

REFERENCES

1. Noll, K.E.; Gournaris, V.; Hou, W.S. (1992) *Adsorption Technology for Air and Water Pollution Control*; Lewis Publishers: Chelsea.
2. Do, D.D. (1998) *Adsorption Analysis, Equilibria and Kinetics*; Imperial College Press: London.
3. Tamai, H.; Yoshida, T.; Sasaki, M.; Yasuda, H. (1999) Dye adsorption on mesoporous activated carbon fiber obtained from pitch containing yttrium complex. *Carbon*, 37: 983–989.
4. Ofomaja, A.E. (2008) Kinetic study and sorption mechanism of methylene blue and methyl violet onto mansonia (Mansonia altissima) wood sawdust. *Chem. Eng. J.*, 143: 85–95.
5. Kumar, K.V.; Sivanesan, S. (2006) Isotherm parameters for basic dyes onto activated carbon: Comparison of linear and non-linear method. *J. Hazard. Mater.*, B129: 147–150.
6. Janoš, P.; Michálek, P.; Turek, L. (2007) Sorption of ionic dyes onto untreated low–rank coal–oxihumolite: a kinetic study. *Dyes Pigm.*, 74: 363–370.
7. Teng, H.; Hsieh, C.T. (1998) Influence of surface characteristics on liquid–phase adsorption of phenol by activated carbons prepared from bituminous coal. *Ind. Eng. Chem. Res.*, 37: 3618–3624.
8. Hsieh, C.T.; Teng, H. (2000) Langmuir and Dubinin–Radushkevich analyses on equilibrium adsorption of activated carbon fabrics in aqueous solutions. *J. Chem. Technol. Biotechnol.*, 75: 1066–1072.
9. Ying, W.C. (1989) *Proceedings of the 44th Purdue Industrial Waste Conference*; Lewis Publishers: Chelsea, Michigan, 313–324.
10. Eswaramoorthy, M.; Sen, R.; Rao, C.N.R. (1999) A study of micropores in single–walled carbon nanotubes by the adsorption of gases and vapors. *Chem. Phys. Lett.*, 304: 207–210.
11. Li, Y.H.; Wang, S.; Zhang, X.; Wei, J.; Xu, C.; Luan, Z.; Wu, D. (2003) Adsorption of fluoride from water by aligned carbon nanotubes. *Mater. Res. Bull.*, 38: 469–476.
12. Peng, X.; Li, Y.; Luan, Z.; Di, Z.; Wang, H.; Tian, B.; Jia, Z. (2003) Adsorption of 1,2–dichlorobenzene from water to carbon nanotubes. *Chem. Phys. Lett.*, 376: 154–158.
13. Hsieh, C.T.; Chen, J.M.; Kuo, R.R.; Huang, Y.H. (2004) Fabrication of well–aligned carbon nanofiber array and its gaseous–phase adsorption behavior. *Appl. Phys. Lett.*, 84: 1186–1188.
14. Hsieh, C.T.; Lin, Y.T.; Lin, J.Y.; Wei, J.L. (2009) Synthesis of carbon nanotubes over Ni-and Co–supported $CaCO_3$ catalysts using catalytic chemical vapor deposition. *Mater. Chem. Phys.*, 114: 702–708.
15. Hsieh, C.T.; Lin, Y.T.; Lin, J.Y.; Wei, J.L. (2009) Parameter setting on growth of carbon nanotubes over transition metal/alumina catalysts in a fluidized bed reactor. *Powder Technol.*, 192: 16–22.
16. Teng, H.; Hsieh, C.T. (1999) Liquid–phase adsorption of phenol by activated carbons prepared from bituminous coals with different oxygen contents. *J. Chem. Technol. Biotechnol.*, 74: 123–130.
17. Hsieh, C.T.; Teng, H. (2000) Liquid–phase adsorption of phenol onto activated carbons prepared with different activation levels. *J. Colloid Interface Sci.*, 230: 171–175.
18. Hsieh, C.T.; Teng, H. (2000) Influence of mesopore volume and adsorbate size on adsorption capacities of activated carbons in aqueous solutions. *Carbon*, 38: 863–869.
19. Lin, S.H.; Hsu, F.M. (1995) Liquid–phase adsorption of organic compounds by granular activated carbon and activated carbon fibers. *Ind. Eng. Chem. Res.*, 34: 2110–2116.
20. Sakoda, A.; Kawazoe, K.; Suzuki, M. (1987) Adsorption of tri– and tetra–chloroethylene from aqueous solutions on activated carbon fibers. *Water Res.*, 21: 717–722.
21. Sakoda, A.; Suzuki, M.; Hirai, R.; Kawazoe, K. (1991) Trihalomethane adsorption on activated carbon fibers. *Water Res.*, 25: 219–225.
22. Yang, O.B.; Kim, J.C.; Lee, J.S.; Kim, Y.G. (1993) Use of activated carbon fiber for direct removal of iodine from acetic acid solution. *Ind. Eng. Chem. Res.*, 32: 1692–1697.

23. Hsieh, C.T.; Chen, W.Y.; Lin, J.H. (2009) Synthesis of carbon nanotubes on carbon fabric for use as electrochemical capacitor. *Microporous Mesoporous Mater.*, 122: 155–159.
24. Hsieh, C.T.; Chen, W.Y.; Wu, F.L. (2008) Fabrication and superhydrophobicity of fluorinated carbon fabrics with micro/nanoscaled two–tier roughness. *Carbon*, 46: 1218–1224.
25. Hsieh, C.T.; Chou, Y.W.; Lin, J.Y. (2007) Fabrication and electric capacitive behavior of hetero–junction carbon nanoclusters by using secondary chemical vapor deposition. *Chem. Phys. Lett.*, 444: 149–154.
26. McKay, G.; Bino, M.J.; Altamemi, A.R. (1985) The adsorption of various pollutants from aqueous solution on to activated carbon. *Water Res.*, 19: 491–495.
27. Krungleviciute, V.; Heroux, L.; Migone, A.D.; Kingston, C.T.; Simard, B. (2005) Isosteric heat of argon adsorbed on single–walled carbon nanotubes prepared by laser ablation. *J. Phys. Chem. B*, 109: 9317–9320.
28. Ansón, A.; Jagiello, J.; Parra, J.B.; Sanjuán, M.L.; Benito, A.M.; Maser, W.K.; Martínez, M.T. (2004) Porosity, surface area, surface energy and hydrogen adsorption in nanostructured carbons. *J. Phys. Chem. B*, 108: 15820–15826.
29. Pariente, S.; Trens, P.; Fajula, F.; Renzo, F.D.; Tanchoux, N. (2006) Heterogeneous catalysis and confinement effects: The isomerization of 1–hexene on MCM–41 materials. *Appl. Catal., A*, 307: 51–57.
30. Babaa, M.R.; Dupont–Pavlovsky, N.; McRac, E.; Masenelli–Varlot, K. (2004) Physical adsorption of carbon tetrachloride on as–produced and on mechanically opened single walled carbon nanotubes. *Carbon*, 42: 1549–1554.
31. Yang, S.; Li, J.; Shao, D.; Hu, J.; Wang, X. (2009) Adsorption of Ni(II) on oxidized multi-walled carbon nanotubes: effect of contact time, pH, foreign ions and PAA. *J. Hazard. Mater.*, 166: 109–116.
32. Hasany, S.M.; Saeed, M.M. (1992) A kinetic and thermodynamic study of silver sorption onto manganese dioxide from acid solutions. *Sep. Sci. Technol.*, 27: 1789–1800.
33. Hobson, J.P. (1969) Physical adsorption isotherms extending from ultrahigh vacuum to vapor pressure. *J. Phys. Chem.*, 73: 2720–2727.
34. Reid, R.C.; Prausnitz, J.M.; Poling, B.E. (1987) *The Properties of Gases and Liquids*; McGraw–Hill: Singapore.
35. Yan, X.M.; Shi, B.Y.; Lu, J.J.; Feng, C.H.; Wang, D.S.; Tang, H.X. (2008) Adsorption and desorption of atrazine on carbon nanotubes. *J. Colloid Interface Sci.*, 321: 30–38.
36. Xie, X.; Gao, L.; Sun, J. (2007) Thermodynamic study on aniline adsorption on chemical modified multi–walled carbon nanotubes. *Colloids Surf. A*, 308: 54–59.